SCIENTIFIC REP♦RTS

OPEN # Omni-resonant optical micro-cavity

Soroush Shabahang[1], H. Esat Kondakci [1], Massimo L. Villinger[1], Joshua D. Perlstein[2], Ahmed El Halawany[1] & Ayman F. Abouraddy[1,2]

Optical cavities transmit light only at discrete resonant frequencies, which are well-separated in micro-structures. Despite attempts at the construction of planar 'white-light cavities', the benefits accrued upon optically interacting with a cavity – such as resonant field buildup – have remained confined to narrow linewidths. Here, we demonstrate achromatic optical transmission through a planar Fabry-Pérot micro-cavity via angularly multiplexed phase-matching that exploits a bio-inspired grating configuration. By correlating each wavelength with an appropriate angle of incidence, a continuous spectrum resonates and the micro-cavity is rendered transparent. The locus of a single-order 0.7-nm-wide resonance is de-slanted in spectral-angular space to become a 60-nm-wide achromatic resonance spanning multiple cavity free-spectral-ranges. The result is an 'omni-resonant' planar micro-cavity in which light resonates continuously over a broad spectral span. This approach severs the link between the resonance bandwidth and the cavity-photon lifetime, thereby promising resonant enhancement of linear and nonlinear optical effects over broad bandwidths in ultrathin devices.

Optical cavities are a cornerstone of photonics[1]. They are indispensable in lasers, optical filters, optical combs[2] and clocks[3], in quantum physics[4], and have enabled the detection of gravitational waves[5]. Optical-cavity resonances occupy narrow spectral linewidths that are inversely proportional to the cavity-photon lifetime, which are separated by a free spectral range (FSR) that is inversely proportional to the cavity size. Although cavity-quantum electrodynamics requires narrow cavity linewidths to isolate the interaction of optical fields with the resonances of atoms, ions, or nanostructures[4], most applications would benefit from maintaining the resonant cavity-field-buildup over an extended bandwidth. Examples of such applications include coherent perfect absorption (CPA) in media endowed with low intrinsic losses[6,7] and boosting nonlinear optical effects[8]. Although CPA, for instance, can increase absorption to 100% in a thin low-loss layer *on* resonance[9,10], exploiting CPA in harvesting solar radiation would require an optical cavity in which an *extended bandwidth* satisfies the resonance condition.

The quest for producing an achromatic resonator has precedents. In 'white-light cavities', the cavity itself is modified by inserting a new material or structure endowed with strong negative (anomalous) dispersion to equalize the cavity optical length for all wavelengths[11]. Only macroscopic white-light cavities have been explored to date via cavity-filling atomic species featuring bifrequency Raman gain in a double-λ system[12] or displaying electromagnetically induced transparency[13], or alternatively via nonlinear Brillouin scattering[14]. In all such studies, the enhanced cavity linewidths are extremely narrow ($\sim$100 MHz or $<$1-pm-wide) by virtue of the very nature of the atomic or nonlinear resonances utilized, and are limited by uncompensated higher-order dispersion terms. Alternative approaches based on the use of *linear* optical components, such as appropriately designed chirped mirrors[15] or grating pairs[16], have been investigated. Surprisingly, both of these possibilities fail at producing a white-light cavity due to subtle overlooked aspects in the constraints imposed by causality on non-dissipative systems[17,18]. A different approach in the context of whispering gallery modes in a micro-cavity relies on increasing the modal density by enlarging the cavity volume[19,20]. First, increasing the cavity diameter reduces the free-spectral range (by increasing the number of modes identified by the azimuthal index) while retaining the high cavity finesse; and, second, the enlarged cavity thickness introduces new modes in the orthogonal dimension. The combination of the resonances of different spatial modes creates a flat spectral response by virtue of their spectral overlap upon proper coupling of light to the cavity[19,20].

Here we demonstrate achromatic transmission through a planar Fabry-Pérot micro-cavity – *not* via a modification of its structure, but instead by altering the spectral-angular configuration of the incident optical radiation using linear optical components. We show that the spatial degree-of-freedom of the optical field when used *in conjunction* with its spectral degree-of-freedom altogether obviates the limitations inherent in

[1]CREOL, The College of Optics & Photonics, University of Central Florida, Orlando, Florida, 32816, USA. [2]Materials Science and Engineering Department, College of Engineering and Computer Science, University of Central Florida, Orlando, FL, 32816, USA. Correspondence and requests for materials should be addressed to A.F.A. (email: raddy@creol.ucf.edu)
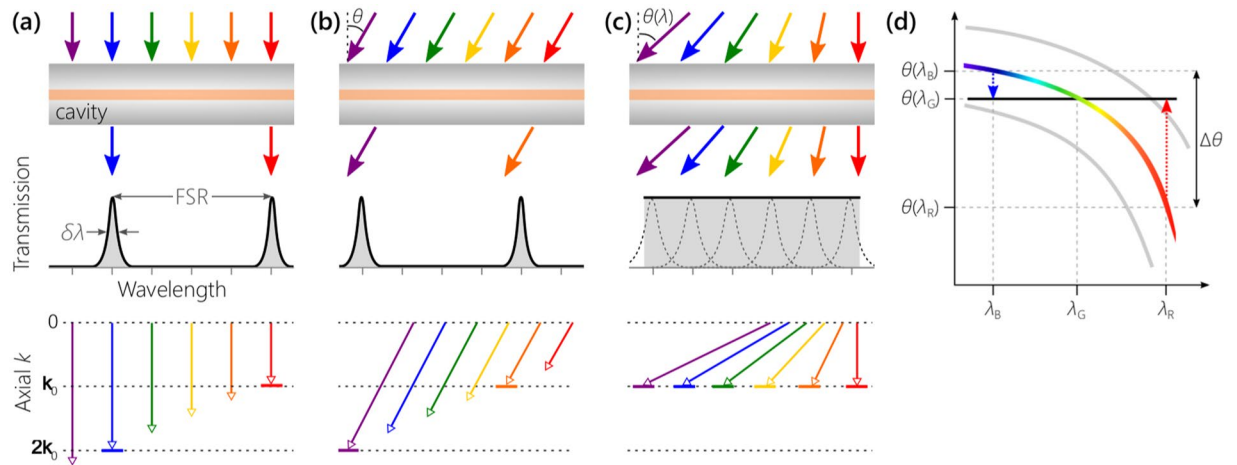
Figure 1. Spectral-angular correlations produce achromatic resonances in a micro-cavity. (**a**) When collimated broadband light is incident normally on a planar Fabry-Pérot cavity (top row), only a discrete set of wavelengths transmit (middle row) whose axial component of the wave vector inside the cavity is an integer multiple of $k_o = \pi/d$ (identified by solid horizontal dashes in the bottom row); $\delta\lambda$ is the resonance linewidth. (**b**) The cavity resonances are blue-shifted when light is incident at an angle θ. (**c**) By assigning each wavelength λ to an appropriate angle of incidence $\theta(\lambda)$, all the wavelengths can resonate and transmission becomes achromatic. One resonant order can extend here over a bandwidth exceeding the FSR. (**d**) Locus of resonant orders in spectral-angular space. Fixing the angle of one wavelength $\theta(\lambda_G)$, we can de-slant the resonance of a specific order (colored curve) by boosting and reducing a pre-compensation angle for each wavelength to produce an achromatic resonance (solid horizontal line). An angular spread $\Delta\theta$ at the input is required to de-slant the resonance between λ_B and λ_R. At the shorter wavelength λ_B, the incidence angle needs to be increased above $\theta(\lambda_G)$ by $\theta(\lambda_B) - \theta(\lambda_G)$. The longer wavelength λ_R requires an incidence angle lower than $\theta(\lambda_G)$ by $\theta(\lambda_G) - \theta(\lambda_R)$. Consequently, λ_R, λ_G, and λ_B all satisfy the resonance condition.

traditional approaches to constructing a white-light cavity. In place of narrow well-separated resonant linewidths of a micro-cavity, broadband 'achromatic resonances' emerge. Starting from the curved locus of a cavity resonance in spectral-angular space, we *de-slant* this locus through angular multiplexing of incident broadband light. Achromaticity is achieved by establishing a judicious correlation between the wavelengths and their associated incident angles, which results in optical 'clearing' of the cavity. Anomalous angular diffraction – achieved via a bio-inspired grating configuration[21, 22] – engenders the necessary correlation and enables continuous phase-matching of the wave-vector axial component to fulfill the resonance condition over an extended bandwidth. The result is thus an 'omni-resonant' optical micro-cavity, whereupon wavelengths are simultaneously and continuously resonant across a large bandwidth. We demonstrate this effect using a planar micro-cavity whose linewidth is $\approx$0.7-nm-wide and FSR is $\approx$25 nm. Single-order $\approx$60-nm-wide resonances that span multiple original FSRs emerge, thereby rendering the resonator transparent – and even enabling the formation of an image through it. In principle, such achromatic resonances can be established over an indefinitely wide bandwidth by replacing the grating with an appropriately designed metasurface[23].

The concept of an achromatic resonance

The underlying physical principle for realizing an omni-resonant planar Fabry-Pérot cavity can be understood by referring to Fig. 1. At normal incidence [Fig. 1a], only discrete wavelengths resonate whose associated roundtrip phase φ is an integer multiple of 2π, $\varphi(\lambda) = 2nkd + 2\gamma(\lambda) = 2\pi m$; here λ is the free-space wavelength, $k = 2\pi/\lambda$ is the wave number, d and n are the thickness and refractive index of the cavity layer, respectively, integer m is the resonant-mode order, and γ is the reflection phase from the cavity mirrors[1] (assumed symmetric). At an incidence angle θ, the resonances are *blue-shifted* [Fig. 1b] because only the *axial* component of the wave vector contributes to the phase $\varphi(\lambda, \theta) = 2nkd \cos\theta' + 2\gamma(\lambda, \theta') = 2\pi m$, where θ' is the angle inside the cavity corresponding to an external angle θ. Indeed, for every wavelength λ, there is an angle $\theta(\lambda)$ that enables this particular wavelength to resonate by satisfying the phase-matching condition

$$\varphi(\lambda, \theta) = 2nkd \cos[\theta'(\lambda)] + 2\gamma(\lambda, \theta') = 2\pi m. \tag{1}$$

Therefore, re-organizing the incident broadband radiation by assigning each wavelength λ to an appropriate incidence angle $\theta(\lambda)$ enables all the angularly multiplexed wavelengths to resonate simultaneously [Fig. 1c], with shorter wavelengths requiring larger incidence angles. Hence, by providing a pre-compensation tilt angle to each wavelength prior to incidence, such that $k \cos[\theta'(\lambda)]$ is constant, we effectively de-slant the resonance by maintaining $\varphi(\lambda, \theta)$ independent of λ [the horizontal line in Fig. 1d].

We first present a heuristic argument for the construction of an optical system that de-slants a resonance in spectral-angular space [Fig. 2a]. A 'black box' system that implements any of the targeted correlations $\theta(\lambda)$ shown
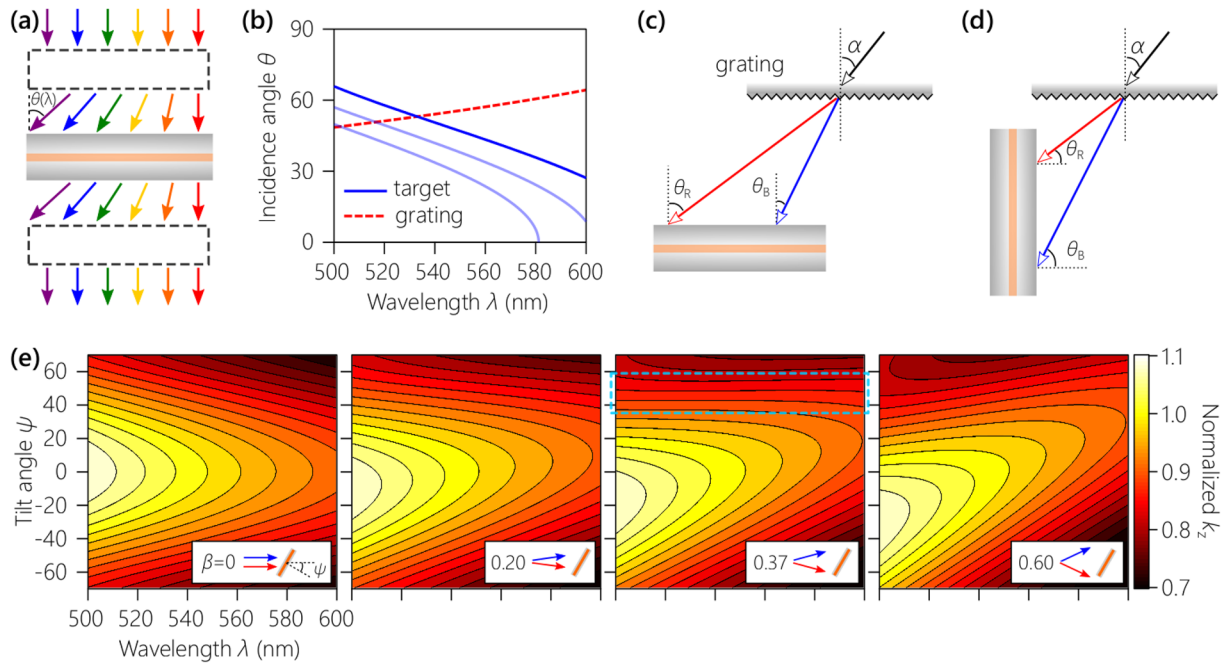
Figure 2. Concept of angularly multiplexed phase-matching to produce an omni-resonant cavity. (**a**) Using an appropriate 'black-box system correlating λ with θ [as in Fig. 1c], a planar micro-cavity is rendered transparent. The inverse of this system is placed after the cavity to restore the original beam. (**b**) The solid curves are target correlations between λ and θ that help de-slant different resonant mode-orders in a planar micro-cavity [corresponding to the highlighted resonances in Fig. 3d]. The dashed curve corresponds to the correlation imparted to a collimated broadband beam centered at $\lambda_c = 550$ nm that is incident normally on a planar surface grating having 1800 lines/mm. (**c**) Angular diffraction resulting from a planar surface grating parallel and (**d**) normal to the plane of a cavity. The former configuration produces the grating curve in (**b**) when $\alpha = 0$. (**e**) Calculated $k_z(\lambda, \psi)$ normalized with respect to $k_c = n\frac{2\pi}{\lambda_c}$ in a planar layer of index $n = 1.5$. The highlighted region in the third panel where $\beta = 0.37°$/nm is independent of λ and thus can support achromatic resonances. Insets in each panel in (**e**) depict the corresponding configurations of broadband light incident on the planar layer.

in Fig. 2b will enable a broadband beam to transmit through the cavity via angular multiplexing – with all the wavelengths resonating simultaneously – and then its inverse restores the original beam. Dispersive prisms do not provide the required angular spread, and planar surface gratings produce the opposite correlation: longer wavelengths diffract at larger angles with respect to the normal as a consequence of transverse phase-matching [dashed curve in Fig. 2b][24]. In other words, the spatial-spectral dispersion inculcated by an optical grating and by a cavity are in opposition. Instead, so-called 'anomalous diffraction' or 'reverse-color sequence' is required. To address this challenge, we take our inspiration from the reverse-color sequence observed in the diffraction of white light off the wing scales of the butterfly *Pierella luna*[21]. This effect has been revealed to be *geometric* in nature: 'vertical' micro-gratings that grow on the *Pierella luna* scales reverse the sequence of diffracted colors as confirmed by fabricated artificial counterparts[22]. We adopt this strategy here in reflection mode and vary the relative tilt between the grating and the cavity, from 0° in Fig. 2c to 90° in Fig. 2d, to enable a transition from normal to anomalous diffraction, respectively.

To gain insight into the resonance de-slanting procedure, we first examine the spectral-angular variation in the axial wave-vector component k_z of broadband light propagating in a bulk planar layer of refractive index n. Consider a bandwidth $\Delta\lambda$ centered at λ_c and each wavelength is directed at a different angle $\theta(\lambda)$, with $\theta(\lambda_c) = \psi$, such that the beam occupies an angular spread $\Delta\lambda$ (assume the wavelengths are distributed uniformly around ψ). For a wavelength λ incident at an external angle θ, k_z in the layer is

$$k_z(\lambda, \psi; \beta) = \frac{2\pi}{\lambda}\sqrt{n^2 - \sin^2[\psi - \beta(\lambda - \lambda_c)]},$$

(2)

where $\beta = \Delta\theta/\Delta\lambda°$/nm is the angular dispersion, we take $n = 1.5$ and $\lambda_c = 550$ nm, and we ignore the spectral variation of n for simplicity. We search for a region in (λ, ψ) space where k_z is *independent* of λ. We plot in Fig. 2e the value of k_z for several values of angular dispersion β. When mirrors sandwich a layer of thickness d, resonances are established whenever k_z is an integer multiple of π/d. Setting $\beta = 0$, we retrieve the case of collimated light incident on a planar layer at an external angle of incidence ψ. As β increases, the constant-k_z contours display less curvature with respect to λ. At $\beta = 0.37°$/nm we reach a critical condition where k_z over an extended region in (λ, ψ) space becomes *independent* of λ. A broadband optical beam prepared in this configuration will
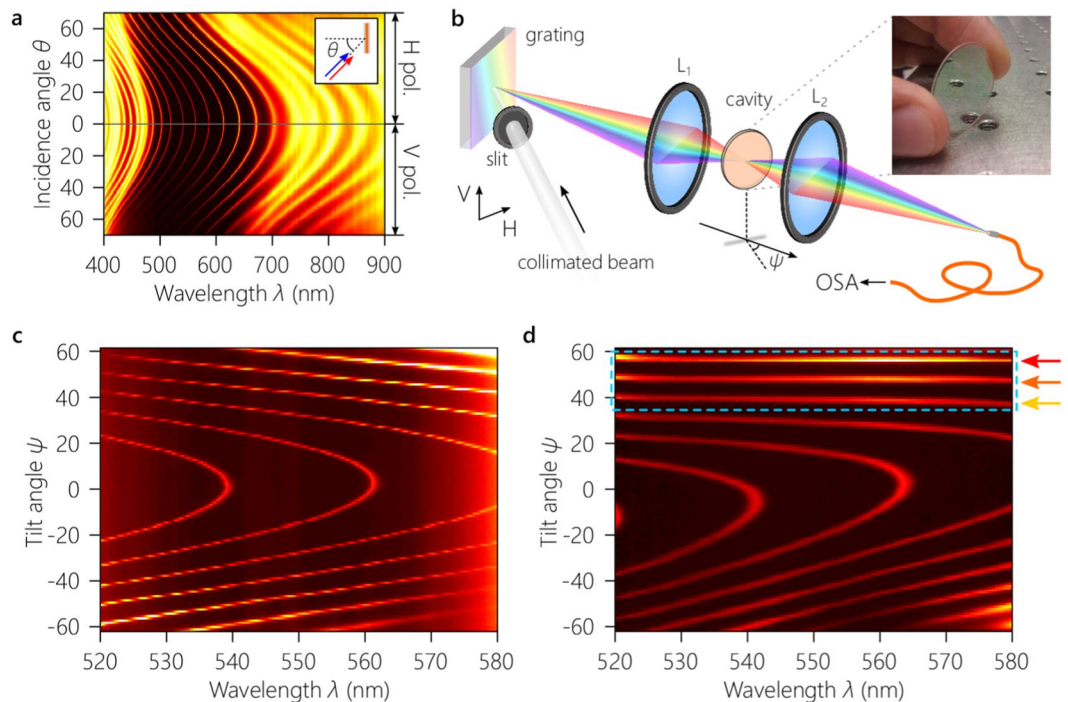
Figure 3. Experimental demonstration of an omni-resonant Fabry-Pérot micro-cavity. (**a**) Measured spectral transmission of collimated light through the cavity with angle of incidence θ for both polarizations. The transmission is symmetric in θ for TE (H: horizontal) and TM (V: vertical) polarizations, so measurements for only positive θ are plotted. Inset is a schematic of the configuration. (**b**) Experimental setup. L_1 and L_2 are lenses, OSA: optical spectrum analyzer; see main text and Supplement 1 for details. Inset is a photograph of the resonator showing strong reflectivity in the visible (cavity sample diameter is 25 mm). (**c**) Measured spectral transmission through the cavity with tilt angle ψ when the focal length of L_1 is $f = 50$ mm. Although the blue-shift with ψ has been enhanced with respect to that in (**a**), the resonances have not been completely de-slanted and thus remain chromatic. (**d**) Measured spectral transmission as in (**c**), except that the focal length of L_1 is $f = 25$ mm. The highlighted resonances are completely de-slanted and are now achromatic over the bandwidth shown. The grating and lens L_1 realize the target $\theta(\lambda)$ correlation functions in Fig. 2b at the three highlighted tilt angles. The measurements in (**c**) and (**d**) are obtained for the H polarization in 1° steps for ψ.

transmit through an omni-resonant cavity via an achromatic resonance supported in this region. Increasing β further reverses the curvature of the constant-k_z contours with respect to λ, thereby disrupting the achromatic resonances.

Experiment

We have carried out an experiment to confirm this prediction of achromatic resonances utilizing a Fabry-Pérot cavity consisting of a 4-μm-thick layer of SiO_2 ($n = 1.48$ at $\lambda = 550$ nm) sandwiched between two Bragg mirrors each formed of 5 bilayers. Each bilayer comprises 92.2-nm and 65.5-nm-thick layers created by the evaporation of SiO_2 and Ti_2O_3 ($n = 2.09$ at $\lambda = 550$ nm), respectively, to produce a 120-nm-wide reflection band with $\approx$92% reflectivity at its center wavelength $\lambda_c \approx 550$ nm at normal incidence. The cavity (total thickness $\approx$5.6 μm) is deposited monolithically by electron-beam evaporation on a 0.5-mm-thick, 25-mm-diameter glass slide [Fig. 3b, inset]. Figure 3a depicts the measured spectral-angular transmission through the cavity obtained using a $\approx$3-mm diameter collimated white-light beam from a halogen lamp revealing the standard behavior of a planar micro-cavity[25]. Upon normal incidence, a finite set of resonant wavelengths are transmitted with a FSR of $\approx$25 nm, which are blue-shifted with angle of incidence θ; see Supplement 1 for details.

We next modify the collimated white-light beam to produce the necessary condition to de-slant the resonance locus – without altering the cavity itself in any way. The beam is first spatially filtered through a 1-mm-wide vertical slit (to avoid aliasing of multiple resonance orders) and is then diffracted from a reflective grating with 1800 lines/mm Fig. 3b]. The grating produces an angular dispersion of $\beta \approx 0.09°$/nm at $\lambda_c = 550$ nm. A grating with $\approx$3500 lines/mm produces the target β, but such a high-density grating has a low diffraction-efficiency in the visible. To enhance β, we add a lens in the path of the diffracted beam before the cavity [L_1 in Fig. 3b]. The spectral transmission through the Fabry-Pérot cavity with tilt angle ψ is plotted in Fig. 3c,d. It is critical to note that the angle ψ is *not* the incidence angle of the beam onto the cavity, but is instead simply the tilt angle of the cavity with respect to the central wavelength $\lambda_c = 550$ nm that defines the optical axis (see Supplement 1); each wavelength is in fact incident at its own angle $\theta(\lambda)$. For convenience, we hold the grating fixed and rotate the cavity. Using L_1 with focal length $f = 50$ mm, β is enhanced to 0.13°/ nm, and the blue-shift of the resonance loci is boosted
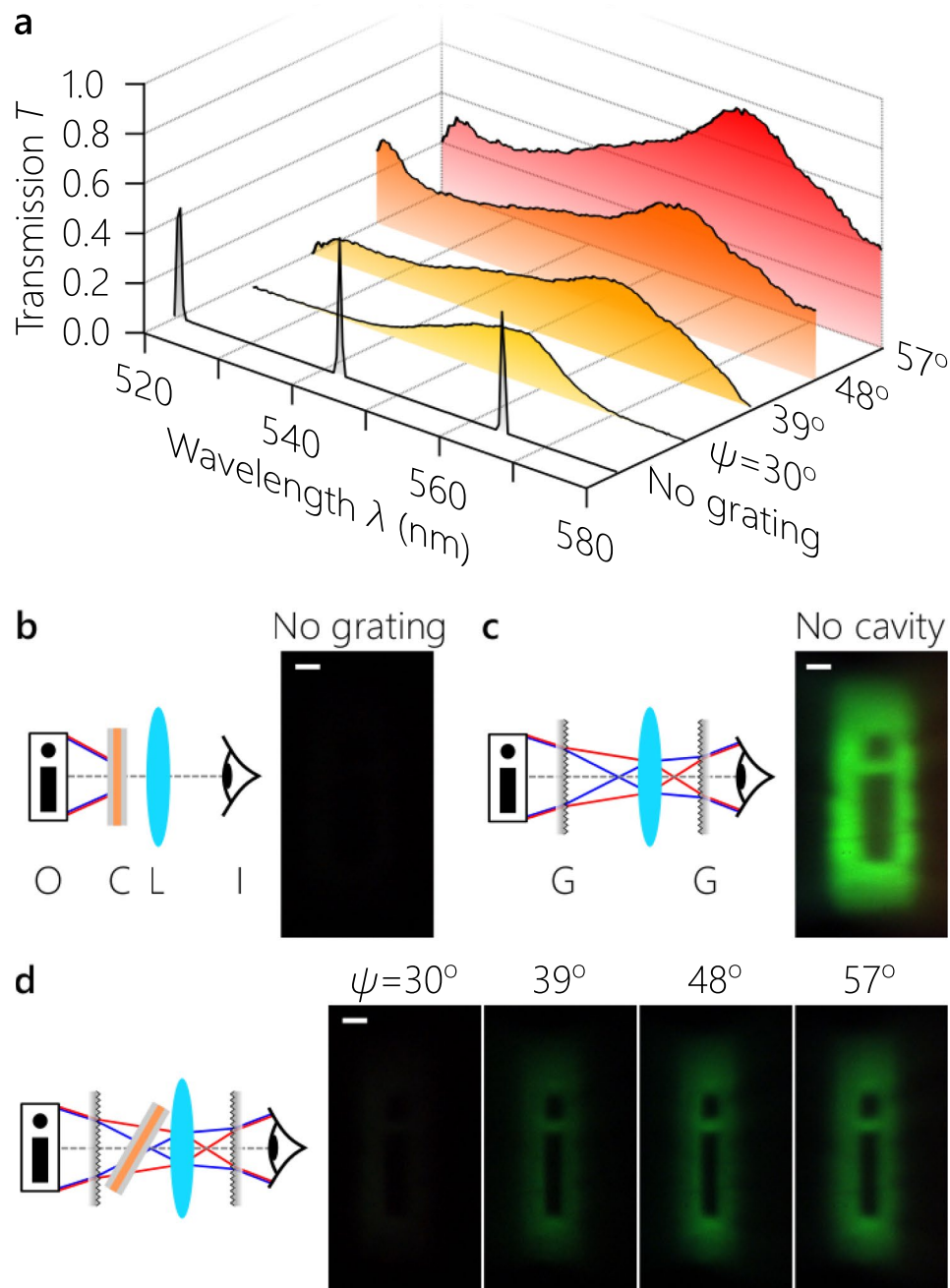
Figure 4. Imaging through an omni-resonant cavity. (**a**) Measured spectral transmission for the achromatic resonances highlighted in Fig. 3d. We also plot the measured bare-cavity normal-incidence transmission (in absence of gratings). (**b**) Imaging an object through the cavity. The image is not visible because light is transmitted only through narrow resonances corresponding to the 'No grating' condition in (**a**). (**c**) Imaging an object in absence of the cavity. Here all the source spectrum contributes to the image. (**d**) Imaging an object through achromatic resonances at the angular settings depicted in (**a**). On the left of the panels (**b**–**d**) we illustrate the imaging configuration and on the right we display the CCD image; scale bars are all 250 μm. O: object plane, C: cavity, L: imaging lens, I: image plane (location of the CCD camera), G: grating; see Supplement 1 for details. The CCD camera gain is held fixed throughout the measurements.

[Fig. 3c]. Reducing the focal length of L_1 to $f = 25$ mm increases β further and reaches the desired angular/spectral dispersion [corresponding to the third panel in Fig. 2e]. The resonance loci are now flattened horizontally at specific values of ψ, whereupon all the wavelengths extending across a 60-nm-wide bandwidth – exceeding twice the FSR – resonate simultaneously [Fig. 3d], a phenomenon we name achromatic resonance.

As a result of the omni-resonant nature of the cavity, one may indeed image an object through it with broadband illumination. We add a lens to the setup in Fig. 3b to image a plane preceding the grating to a plane lying

beyond the cavity (see Supplement 1). The object is a binary-valued 0.25×2 mm^2 transparency of the letter 'i' that is imaged through the cavity with a magnification factor of ≈ 3. In absence of the grating, a limited amount of light is transmitted through the cavity at any incident angle due to the large FSR and narrow linewidth of the resonances lying within the cavity mirror bandgap [Fig. 4a,b] – when compared to the configuration where the cavity is absent [Fig. 4c]. In presence of the grating that renders the cavity transparent, a substantial amount of light is transmitted when the cavity tilt angle corresponds to that of an achromatic resonance: at $\psi = 30°$, 39°, 48°, and 57° [Fig. 4a,d].

Conclusion

Our proof-of-principle experiment of an omni-resonant optical cavity renders transparent a micro-cavity with 0.7-nm-wide resonances separated by an FSR of ≈ 25 nm, thanks to an achromatic resonance operating continuously over a broad spectrum (≈ 60 nm). Our approach is analogous to that of refs 19, 20. and relies on the same principle: coupling each spectral component of the input field to a particular spatial mode matching the resonance condition. In refs 19, 20 the set of spatial modes is discrete, whereas the set of spatial modes identified by the wave vectors in the planar cavities explored here spans a continuum.

Although the necessary correlation between wavelength and incidence angle is introduced using a planar surface grating, the bandwidth can be broadened further and the uniformity of the spectral transmission improved by replacing the grating with a metasurface realizing a customized function $\theta(\lambda)$ that takes into account the cavity mirror spectral phase $\gamma(\lambda, \theta)$, its polarization dependence, and wavelength dependence of the refractive index[26]. Furthermore, such a metasurface may indeed implement the reverse-color sequence without introducing a tilt angle with respect to the cavity[27]. Consequently, depositing the metasurface directly on the planar micro-cavity may potentially result in ultra-thin optical devices that deliver resonant linear and nonlinear behavior over extended bandwidths.

We have introduced here a general principle that lifts the bandwidth restrictions associated with resonant linewidths in an optical micro-cavity – leading to the realization of an omni-resonant or white-light cavity. While recent work has exploited spectral splitting of the solar spectrum to optimize the photovoltaic conversion with multiple semiconductor junctions[28], our approach – on the other hand – implements a continuous mapping to a wavelength-dependent angle of incidence $\theta(\lambda)$. Indeed, our work extends to the continuum the correlations between discretized optical degrees of freedom studied in refs 29–31. As a result, the advantages associated with a resonance – such as field enhancement through resonant buildup and enhanced optical nonlinearities – become altogether decoupled from the cavity linewidth and are thus available over orders-of-magnitude larger bandwidths. This concept can have a profound impact on optics by bringing coherent perfect absorption to bear on harvesting solar energy, producing white-light micro-lasers, and yielding broadband resonantly enhanced nonlinear optical devices.

References

1. Saleh, B. E. A. & Teich, M. C. *Fundamentals of Photonics* (Wiley, 2007).
2. Pfeifle, J. *et al*. Coherent terabit communications with microresonator kerr frequency combs. *Nat. Photonics* **8**, 375–380 (2014).
3. Diddams, S. A. *et al*. An optical clock based on a single trapped ^{199}Hg$^+$ ion. *Science* **293**, 825–293 (2001).
4. Haroche, S. & Raimond, J.-M. *Exploring the Quantum: Atoms, Cavities, and Photons* (Oxford, 2006).
5. Abbott *et al*. B. P. LIGO: The laser interferometer gravitational-wave observatory. *Rep. Prog. Phys.* **72**, 076901 (2009).
6. Chong, Y. D., Ge, L., Cao, H. & Stone, A. D. Coherent perfect absorbers: Time-reversed lasers. *Phys. Rev. Lett.* **105**, 053901 (2010).
7. Wan, W. *et al*. Time-reversed lasing and interferometric control of absorption. *Science* **331**, 889–892 (2011).
8. Makri, E., Ramezani, H., Kottos, T. & Vitebskiy, I. Concept of a reflective power limiter based on nonlinear localized modes. *Phys. Rev. A* **89**, 031802(R) (2014).
9. Villinger, M. L., Bayat, M., Pye, L. N. & Abouraddy, A. F. Analytical model for coherent perfect absorption in one-dimensional photonic structures. *Opt. Lett.* **40**, 5550–5553 (2015).
10. Pye, L. N. *et al*. Octave-spanning coherent absorption in a thin silicon film. *Opt. Lett.* **42**, 151–154 (2017).
11. Wicht, A. *et al*. White-light cavities, atomic phase coherence, and gravitational wave detectors. *Opt. Commun.* **134**, 431–439 (1997).
12. Pati, G. S., Salit, M., Salit, K. & Shahriar, M. S. Demonstration of a tunable-bandwidth white-light interferometer using anomalous dispersion in atomic vapor. *Phys. Rev. Lett.* **99**, 133601 (2007).
13. Wu, H. & Xiao, M. White-light cavity with competing linear and nonlinear dispersions. *Phys. Rev. A* **77**, 031801(R) (2008).
14. Yum, H. N., Sheuer, J., Salit, M., Hemmer, P. R. & Shahriar, M. S. Demonstration of white light cavity effect using stimulated Brillouin scattering in a fiber loop. *J. Lightwave Technol.* **32**, 3865–3872 (2013).
15. Szipöcs, R., Ferencz, K., Spielmann, C. & Krausz, F. Chirped multilayer coatings for broadband dispersion control in femtosecond lasers. *Opt. Lett.* **19**, 201–203 (1994).
16. Wise, S., Mueller, G., Reitze, D., Tanner, D. B. & Whiting, B. F. Linewidth-broadened fabryperot cavities within future gravitational wave detectors. *Class. Quantum Grav.* **21**, S1031–S1036 (2004).
17. Yum, H. N., Liu, X., Hemmer, P. R., Scheuer, J. & Shahriar, M. S. The fundamental limitations on the practical realizations of white light cavities. *Opt. Commun.* **305**, 260–266 (2013).
18. Wise, S. *et al*. Phase effects in the diffraction of light: Beyond the grating equation. *Phys. Rev. Lett.* **95**, 013901 (2005).
19. Savchenkov, A. A., Matsko, A. B. & Maleki, L. White-light whispering gallery mode resonators. *Opt. Lett.* **31**, 92–94 (2006).
20. Strekalov, D. V., Savchenkov, A. A., Savchenkova, E. A. & Matsko, A. B. Trapping light into high orbital momentum modes of fiber tapers. *Opt. Lett.* **40**, 3782–3785 (2015).
21. Vigneron, J. P. *et al*. Reverse color sequence in the diffraction of white light by the wing of the male butterfly *Pierella luna* (nymphalidae: Satyrinae). *Phys. Rev. E* **82**, 021903 (2010).
22. England, G. *et al*. Bioinspired micrograting arrays mimicking the reverse color diffraction elements evolved by the butterfly *Pierella luna*. *Proc. Natl. Acad. Sci. USA* **111**, 15630–15634 (2014).
23. Aieta, F., Kats, M. A., Genevet, P. & Capasso, F. Multiwavelength achromatic metasurfaces by dispersive phase compensation. *Science* **347**, 1342–1345 (2015).
24. Palmer, C. *Diffraction Grating Handbook* (Newport, Rochester, New York, 2005).
25. Yeh, P. *Optical Waves in Layered Media* (Wiley, 2005).
26. Yu, N. & Capasso, F. Flat optics with designer metasurfaces. *Nat. Mater.* **13**, 139–150 (2014).
27. High, A. A. *et al*. Visible-frequency hyperbolic metasurface. *Nature* **522**, 192–196 (2015).

28. Imenes, A. G. & Mills, D. R. Spectral beam splitting technology for increased conversion efficiency in solar concentrating systems: A review. *Sol. Energ. Mat. Sol. Cells* **84**, 19–69 (2004).
29. Kagalwala, K. H., Di Giuseppe, G., Abouraddy, A. F. & Saleh, B. E. A. Bell's measure in classical optical coherence. *Nat. Photonics* **7**, 72–78 (2013).
30. Berg-Johansen, S. *et al.* Classically entangled optical beams for high-speed kinematic sensing. *Optica* **2**, 864–868 (2015).
31. Kagalwala, K. H., Kondakci, H. E., Abouraddy, A. F. & Saleh, B. E. A. Optical coherency matrix tomography. *Sci. Rep.* **5**, 15333 (2015).

Acknowledgements

Author Contributions

S.S. and A.F.A. developed the concepts and directed the research. S.S. performed the optical measurements and analysis. H.E.K. carried out simulations and prepared the figures. M.L.V. and J.D.P. designed the device. All authors analyzed the data. S.S., H.E.K., and A.F.A. wrote the paper with input from the co-authors.

Additional Information

Supplementary information accompanies this paper at doi:10.1038/s41598-017-10429-4

Competing Interests: The authors declare that they have no competing interests.

Publisher's note: Springer Nature remains neutral with regard to jurisdictional claims in published maps and institutional affiliations.